applied sciences

MDPI

Article

CFD–DEM Simulation of Dust Deposition on Solar Panels for Desert Railways

Jinghong Zhang [1,*], Xingcai Li [2,3,*], Juan Wang [2,4] and Li Qiao [5]

[1] Department of Civil Engineering, Yancheng Institute of Technology, Yancheng 224051, China
[2] School of Physics and Electronic-Electrical Engineering, Ningxia Key Laboratory of Intelligent Sensing & Desert Information, Ningxia University, Yinchuan 750021, China
[3] Key Laboratory of Mechanics on Disaster and Environment in Western China, The Ministry of Education of China, Lanzhou University, Lanzhou 730000, China
[4] Office of Academic Affairs, Xinhua College of Ningxia University, Yinchuan 750021, China
[5] Institute of Applied Mechanics, College of Mechanical and Vehicle Engineering, Taiyuan University of Technology, Shanxi Key Laboratory of Materials Strength and Structural Impact, Taiyuan 030024, China
* Correspondence: zhangjh_lzu2013@163.com (J.Z.); nxulixc2011@nxu.edu.cn (X.L.)

Abstract: With the greening of the railway energy supply chain, large-scale photovoltaic power stations will be the best choice to integrate with the railways. Understanding the deposition mechanisms and rules of dust grains on photovoltaic panels is of great guiding significance for the operation of photovoltaic (PV) power stations. In this paper, based on computational fluid dynamics (CFD) combined with the discrete element method (DEM), the dynamic dust deposition process on solar panels was simulated, and the flow field around solar panels and the movement of dust particles in the wind were calculated. The simulation results of clay particles (d = 10 mm) and fine sand particles (d = 100 mm) under different wind speeds showed that the clay particles could follow the air flow properly, and their deposition rate was only 4.6%, while the deposition rate of the fine sand particles was up to 32%, which was determined by the inflow wind speed and cohesion parameters. An image of the non-uniform distribution of particles on the panels was given in this paper for the first time. This will provide a basis for a more accurate assessment of the impact of dust accumulation on PV output in real-world environments. These results provide a critical reference for railway photovoltaic power supply development in desertification areas.

Keywords: photovoltaic power; dust deposition; CFD–DEM method; flow field; cohesion parameters

check for updates

Citation: Zhang, J.; Li, X.; Wang, J.; Qiao, L. CFD–DEM Simulation of Dust Deposition on Solar Panels for Desert Railways. *Appl. Sci.* **2023**, *13*, 4. https://doi.org/10.3390/app13010004

Academic Editor: Alejandro Pérez-Rodríguez

Received: 19 November 2022
Revised: 12 December 2022
Accepted: 13 December 2022
Published: 20 December 2022

Copyright: © 2022 by the authors. Licensee MDPI, Basel, Switzerland. This article is an open access article distributed under the terms and conditions of the Creative Commons Attribution (CC BY) license (https://creativecommons.org/licenses/by/4.0/).

1. Introduction

The scale of China's railway network is the largest in the world, and many of its railways are in the northwest where desertification is severe. In 2022, the Taklimakan desert railway was completed; it was the world's first around-desert railway with a length of 2712 km. In addition, the Baolan railway, Qinghai–Tibet railway, Lanzhou–Xinjiang railway, Golmu–Korla railway and Hami–Lop Nur railway all pass through the desertification zone. The electrification rate of the Chinese railway is nearly 71.9%. As a result, the railway consumes an enormous amount of electricity. In addition, China has the world's largest solar energy power station, and more than half of the solar energy capacity is located in the desertification areas of the northwest of China. With the greening of the railway energy supply chain becoming gradually irreversible, photovoltaic power generation will be the best choice to integrate with railways [1]. However, because of desertification, the impact of atmospheric particulates deposited on photovoltaic (PV) power generation systems has received extensive attention. Some researchers have pointed out that the particles covering PV modules will reduce the efficiency of power generation, thus affecting the normal operation or service life of photovoltaic power generation equipment [2,3]. These particles mainly include clay, dust particles, smoke, pollen and even bird manure. In view of these

conditions, more and more researchers in related fields have carried out studies on the dust accumulation process and power generation efficiency degradation of photovoltaic modules as well as a lot of innovative works in dust removal [4–6].

In recent years, the research on the impact of dust deposition on the power generation efficiency of photovoltaic modules has mainly focused on in-field and indoor experiments. El-Shobokshy [7–9] gave the attenuation curve of solar intensity reduction versus the amount of dust deposition when a solar panel is covered by dust particles with a radius of 80 mm, and the results showed that the radiation intensity decreased to 30% of the original value when the dust amount was 250 g/m^2. Salim et al. [10] pointed out that a solar panel near Saudi Arabia, Riyadh, had a 32% reduction in power generation due to 8 months of dust deposition. Sulaiman et al. [11] carried out indoor experiments with two kinds of artificial dust coverage, and the results showed that the power generation efficiency of dusty solar panels was reduced by 18% compared with clean panels. Kaldellis et al. [12] studied the relationship between dust cover and power generation by artificial sand cover, and they pointed out that power generation efficiency is closely related to the type and size of dust and that the dust deposition is directly proportional to the slope of a solar panel. Darwish et al. [13] studied the impact of pollutant types on the efficiency decline of solar panels and pointed out that it is urgent to establish a model that can reflect the impact of dust types on the efficiency of solar panels. Saidan et al. [14] studied dust deposition on solar panels in an in-field environment and pointed out that the power generation efficiency of solar panels decreased by 6.24% after one day, 11.8% after one week and 18.74% after one month. Generally speaking, the reduction in power generation efficiency is not proportional to the amount of sand dust coverage, which is consistent with the research results of Beattie et al. [15] who found that the area of the dust-free part of the surface of photovoltaic solar panels approximately presents an exponential change through laboratory experiments.

The wind-flow field around a PV module has an important impact on the dust accumulation on the PV module [16]. Some scholars have studied the deposition process of particles based on fluid dynamics models. For example, Jubayer et al. [17] used Reynolds-averaged Navier–Stokes equations to simulate the three-dimensional flow field around a solar panel fixed on the ground, and the results showed that the pressure coefficient was basically consistent with the wind tunnel results proposed by Ogedengbe [18]. Tominaga et al. [19] studied the flow field around a roof solar panel by means of a wind tunnel experiment and a Reynolds-averaged simulation method, and the results showed that the simulation results were in good agreement with the wind tunnel experiment. Ullah et al. [20] found that the tilt angle of a solar panel will affect the amount of dust deposition, resulting in a change in power loss with the tilt angle. Lu et al. [21,22] used the CFD–DPM method to study the flow field and dust deposition around a solar panel installed on the ground, which simulated the trajectory of the sand particles but it was difficult to accurately reflect the rebound, capture and sliding process of the sand particles on the solar panel. Dagher et al. [23] investigate the dust deposition behavior around a ground-mounted solar PV panel with a discrete phase model in CFD simulations, and the influence of the wind speed, dust particle size and dust material on the sand deposition rate were investigated.

In order to understand the law of particle deposition on photovoltaic panels and then to develop efficient dust removal technology, the deposition process of real dust particles on solar panels and the interaction between the dust particles and the panel surface must be simulated accurately, which can be realized by the CFD–DEM method. This method has been applied to some fields [24,25] to simulate the dynamic contact process of individual particles. Therefore, this paper intended to introduce this method to analyze the deposition of atmospheric particles on photovoltaic panels.

This paper is arranged as follows. Section 2 describes the detailed formulas of the CFD–DEM method and the computation conditions. Section 3 introduces the numerical simulation results of the deposited states of the clay and fine particles with different wind speeds and cohesion parameters and the non-uniform concentration distribution of the fine

sand particles deposited on the solar panel due to the rolling movement of sand particles on its surface. Section 4 gives the conclusion. Through the simulation of wind flow and the dust trajectories around the solar panel, the number of deposits could be calculated based on the statistics of the number of particles with zero speed on the solar panel. Then, the deposition difference in the clay and fine sand on the solar panel under different wind speeds was obtained, and the non-uniformity of dust deposition on solar panels was also firstly reported.

2. Coupled CFD-DEM Mathematical Equations

2.1. CFD Equations

The governing equation of the airflow around the solar panel can be expressed by the Reynolds-averaged Navier–Stokes equation, i.e.,

$$\frac{\partial \overline{u}_i}{\partial x_i} = 0 \tag{1}$$

$$\frac{\partial \overline{u}_i}{\partial t} + \overline{u}_j \frac{\partial \overline{u}_i}{\partial x_j} = -\frac{1}{\rho}\frac{\partial \overline{p}}{\partial x_i} + \frac{1}{\rho}\frac{\partial_i}{\partial x_j}\left(\tau_{ij}^m + R_{ij}\right) + f_i \tag{2}$$

where $i,j = 1, 2, 3$, $\overline{u}_i$ is the i-th component of time average velocity, f_i is the i-th component of acceleration, $\boldsymbol{R_{ij}} = -\rho\overline{u_i u_j}$ is Reynolds stress, $\tau_{ij}^m = 2\mu S_{ij}$ is molecular viscosity stress and S_{ij} can be expressed as:

$$S_{ij} = \frac{1}{2}\left(\frac{\partial \overline{u}_i}{\partial x_j} + \frac{\partial \overline{u}_j}{\partial x_i}\right) \tag{3}$$

Equations (1) and (2) is closed by the realizable $k-\varepsilon$ equation, which can be used to describe the boundary-layer-separated flow under a reverse pressure gradient, and the non-equilibrium wall function was used for the boundary flow calculation.

2.2. Dust Particle Trajectory Equation

In this paper, the motion differential equation of the dust particles in air flow can be expressed as:

$$m_i \frac{d\vec{v}_i}{dt} = \vec{f}_{drag,i} + m_i\vec{g} \tag{4}$$

where $\vec{f}_{drag,i}$ is calculated with the free-flow traction model, $\vec{f}_{drag,i} = 0.5C_d\rho_g A_b\left|\vec{v}_{p-a}^{rel}\right|\vec{v}_{p-a}^{rel}$, in which A_b is the projected area of dust particles, $\vec{v}_{p-a}^{rel}$ is the relative velocity between the particles and the air flow and C_d is the drag coefficient, which is calculated from the following formula [26],

$$C_d = \begin{cases} 24/Re & Re \le 0.5 \\ 24(1.0 + 0.15Re^{0.687})/Re, & 0.5 < Re \le 1000 \\ 0.44 & Re > 1000 \end{cases} \tag{5}$$

where Re is the Reynolds number, $Re = \rho_a d_p\left|\vec{v}_{p-a}^{rel}\right|/\mu_a$ and ρ_a, μ_a is the air density and dynamic viscosity coefficient. When particles collide with other particles or solar panels, the contact force between the particles and the other particles or solar panels must be considered. The motion equation of particles can be rewritten as:

$$m_i \frac{d\vec{v}_i}{dt} = \vec{f}_{drag,i} + m_i\vec{g} + \vec{F}_n + \vec{F}_{nd} - \vec{F}_\tau \tag{6}$$

where $\vec{F}_n$, $\vec{F}_{nd}$, $\vec{F}_\tau$ are the normal force, normal damping force and tangent damping force, respectively, which were all calculated by the soft sphere model.

2.3. Contact Model Equations

In this paper, the Hertz–Mindlin nonlinear contact model combined with the linear adhesion model are used to describe the forces between particles with other particles or between particles with the solar panel surface, assuming that the contact between two spheres with radii of R_1 and R_2 is elastic (if the second object is the solar panel surface, R_2 tends to be infinite), and the normal overlap is α, $\alpha = R_1 + R_2 - D_{12}$, where D_{12} is the distance between the centers of two spheres. The contact model is shown in Figure 1. The normal force between particles is $\vec{F}_n$, and its magnitude, F_n, can be expressed as the following [27],

$$F_n = \frac{4}{3}E^*(R^*)^{1/2}\alpha^{3/2} \tag{7}$$

where E^* and R^* are the equivalent modulus of elasticity and the equivalent radius, respectively, which are determined by the following formulas: $1/E^* = \left(1-\nu_1^2\right)/E_1 + \left(1-\nu_2^2\right)/E_2$ and $1/R^* = 1/R_1 + 1/R_2$. Here, E_1, ν_1, E_2, ν_2 are the elastic modulus and Poisson's ratio of two spheres. The magnitude of the normal damping force, $\vec{F}_{nd}$, can be expressed by:

$$F_{nd} = -2\sqrt{\frac{5}{6}}\beta\sqrt{S_n m^*}v_n^{ref} \tag{8}$$

where $\beta = \ln e/\sqrt{\ln^2 e + \pi^2}$, e is the recovery factor, $S_n = 2E^*\sqrt{R^*\alpha}$, $m^* = m_1 m_2/(m_1+m_2)$ is the equivalent mass, and v_n^{ref} is the normal component of relative velocity. In addition, the magnitude of the tangential damping force between particles, $\vec{F}_t$, can be expressed as:

$$F_t = -2\sqrt{\frac{5}{6}}\beta\sqrt{S_t m^*}v_t^{rel} \tag{9}$$

where S_t is the tangential stiffness, $S_t = 8G^*\sqrt{R^*\alpha}$, and G^* is the equivalent shear modulus. Assuming G_1, G_2 are the shear modulus of two spheres, then $1/G^* = \left(2-\nu_1^2\right)/G_1 + \left(2-\nu_2^2\right)/G_2$.

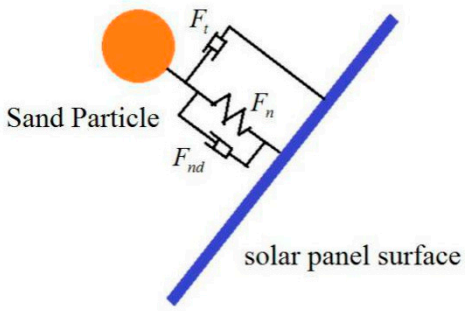


Figure 1. The contact model of dust and solar panel.

In order to describe the cohesion force between the particles and the solar panel, the linear cohesion model was used, which can modify the default Hertz–Mindlin contact model for particle–particle and particle–geometry interactions by adding a normal cohesion force, F_{nc}, which is expressed as:

$$F_{nc} = KA \tag{10}$$

where K is the adhesion energy density, A is the contact area and F_{nc} represents the adhesion between the particles and the solar panel caused by van der Waals forces and electrostatic forces [28], which are difficult to give an accurate calculation method for.

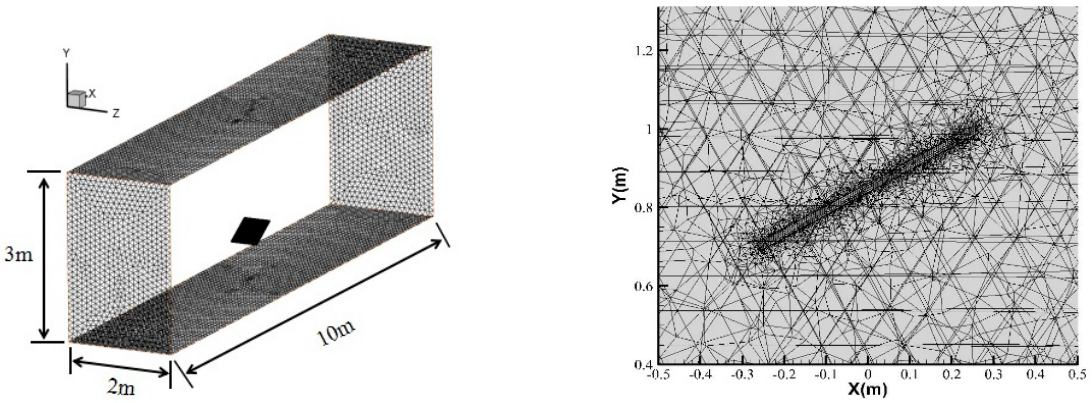
In this study, the effect of the particles volume was neglected because in general dusty weather the mass density of sand/dust particles is relatively small and collisions between particles are rare.

2.4. Flow Region and Model Parameters

The flow region was 10 m × 3 m × 2 m and the size of the solar panel was 0.6 m × 0.5 m × 0.02 m, its installing height was 0.75 m and its inclination was 30°. For the coordinate systems, the x-axis was along the wind flow direction, the y-axis was perpendicular to the ground and the z-axis was towards the span direction, and the origin of the coordinate systems was at the center point of the ground. The grid of the fluid area was tetrahedral with a size of 0.1 m. The grid of the solar panel surface was triangular with a size of 0.005 m, which was small enough to model the solar panel wall flow. The calculation area and grid are shown in Figure 2. A logarithmic velocity profile was used for the inlet boundary condition, which can be expressed as:

$$u(y) = \frac{u_*}{k} \ln \frac{y}{y_0} \tag{11}$$

where u_* is the friction wind velocity and y_0 is the roughness height.



(**a**) (**b**)

Figure 2. Sketch of the numerical model's geometry. (**a**)The simulation zone. (**b**) Modeling grids.

2.5. Adhesion Energy Parameter

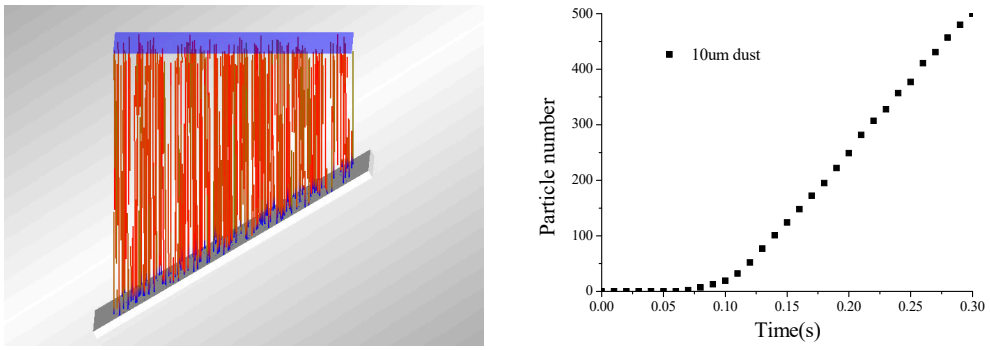
In this research, two types of particles, dust and fine sand, were used for modelling the deposition of particles. The physical parameters of dust particles are shown in Table 1. The cohesion energy parameter, K, between a particle and the solar panel was difficult to determine, so a numerical experiment was designed for testing the above parameter. The numerical experiment used the free settlement of particles from a plane with 20 × 20 cm dimensions above an inclined solar panel with a 30-degree angle. The kinetic deposition process of the particles included three modes of motion in the numerical experiment: complete rebound, partial adhesion and complete adhesion. Since the surface wind speed was approximately zero, the movement of dust was only affected by gravity in the numerical experiments. The deposition of particles with different cohesive forces was calculated, and the release rate of the particles was 2500 particles per second from the PV panels.

Figure 3 shows the deposition process of 10 μm particles, i.e., clay, with $K = 0.5 \times 10^6$ J/m^3. From Figure 3a, it can be seen that the clay particles were almost all deposited on the solar panel because of the cohesiveness between the particles and the solar panel surface, and the results with a much higher value of K were consistent with the above results. The particle number of zero at the first time point (less than 0.075 s) in Figure 3b was because the clay particles were still falling and had not touched the solar panel yet. The deposition simulation results of 100 μm sand particles, i.e., fine sand, on the solar panel were different to those of clay, which would be reflected or deposited with a different cohesiveness. Since the cohesiveness can be indicated by the cohesion energy parameter K, we then calculated the deposition process of fine particles with $K = 0.5 \times 10^6$ J/m^3, 1.05×10^6 J/m^3 and 3.5×10^6 J/m^3, and the results are shown in Figure 4. From Figure 4,

we can see that the falling fine sand particles were difficult to deposit on the solar panel when $K = 0.5 \times 10^6$ J/m^3, while the deposition amount increased as the parameter K increased. Therefore, it is of great significance to characterize the adhesion force between particles and PV panels accurately. Unfortunately, experimental results are rare.

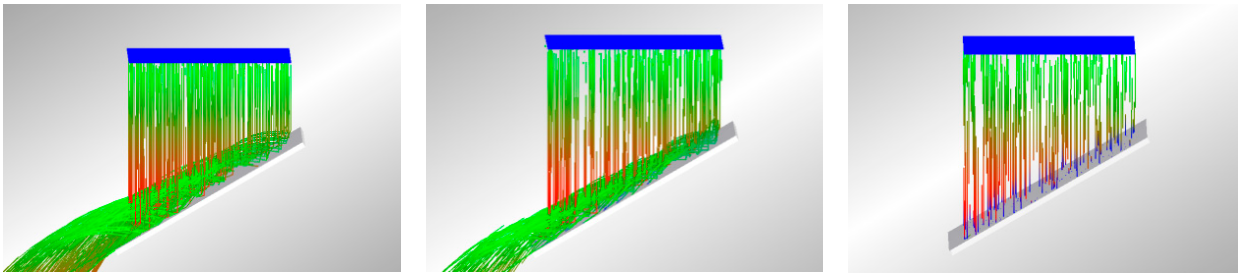
Table 1. Physical parameters of dust particles.

Name	Value
Dust diameter dp_1	0.01 mm
Dust density	2000 kg/m^3
Dust shear modulus G_1	3.5×10^6 Pa
Dust Poisson ratio	0.42
Recovery factor e	0.5
Fine sand diameter dp_2	0.1 mm
Fine sand density	2050 kg/m^3
Fine sand shear modulus G_2	3.0×10^7 Pa
Fine sand Poisson ratio	0.28
Panel glass density	2700 kg/m^3
Panel glass shear modulus G_3	3.0×10^{10} Pa
Panel glass Poisson ratio	0.2



(**a**) (**b**)

Figure 3. (**a**) The deposition of dust particles on the solar panel of 10 um clay particles under static wind with coherent energy parameter $K = 0.5 \times 10^5$ Jm^{-3}, and (**b**) the total number of particles deposited on the solar panel varying with time.



(**a**) (**b**) (**c**)

Figure 4. The deposition of dust particles on the solar panel of 100 μm fine sand particles under static wind with different coherent energy parameters. (**a**) $K = 0.5 \times 10^6$ Jm^{-3}. (**b**) $K = 1.05 \times 10^6$ Jm^{-3}. (**c**) $K = 3.5 \times 10^6$ Jm^{-3}.

3. Numerical Simulation Results and Discussion

3.1. Deposition Characteristics of Dust Particles (Clay) on Solar Panels

The calculation of wind-blown dust/sand flow was a two-step process. First, the steady CFD method was used to calculate the flow field with a fixed friction velocity around the solar panel until the flow field achieved convergence. Second, the transient

CFD method was used to simulate the wind flow including a large number of moving clay particles with a radius 10 μm, whose moving trail, velocity and force were calculated by an EDM method. The release speed of dust particles was along the x-direction with a fixed value of 1.75 m/s, and the calculation time step was as small as 1.25×10^{-7} s, which could prevent dust particles from passing through the surface of the solar panel or sticking inside the panel.

The visibility of typical dusty weather was assumed to be 1 km; then, according to Shao et al. [29], it was estimated that the TSP concentration of the incoming flow was about 2~3 mg/m^3. It was reasonably assumed that the concentration of dust with a diameter of 10 μm is 2 mg/m^3. So, the number of dust particles entering from the entrance section in unit time was

$$N = cUA/m \tag{12}$$

In which $U = 1.75$ m/s, $A = 6$ m^2, $c = 2$ mg/m^3 and $m = 1.152 \times 10^{-6}$ mg. Then, $N = 1.82 \times 10^7$/s. In order to improve the efficiency of the calculation, a ratio of 1:3500 was used for the calculation, that is, the number of released particles at the inlet was 5220/s.

The flow-field contour map of the x-y plane and z-y plane is shown in Figure 5. From Figure 5a, it can be seen that the air flow above the solar panel accelerated gradually along the upper surface because of the wing-flow effect, but the air flow below the solar panel formed a high-speed flow area and a subsequent low-speed zone because of the attack angle of the solar panel and its shading effect, while a low-speed and swirling zones existed, as shown in Figure 5b, behind the solar panel due to the solar panel's blocking of the air flow. In order to better display the particle trajectory around the solar panel, the friction velocity $u_* = 0.25$ ms^{-1}, $K = 0.5 \times 10^6$ J/m^3 and the particle radius was set as 10 μm. The simulation results are shown in Figure 6, in which the rectangular panel is the solar panel, the streamline color represents the magnitude of the dust particle movement speed and the speed range was from 1.21 m/s (blue line) to 2.08 m/s (red line). Compared with Figures 5 and 6, it can be seen that the movement of dust particles followed strongly with the air flow, that is, all the particles above the solar panel almost followed the upward air flow movement and were rarely deposit on the solar panel surface, while below the solar panel, the particles moved around the lower edge of the solar panel at a large speed. Compared with Figures 5b and 6b, after the solar panel, the trajectories of the dust particles were basically consistent with the movement of the air flow vortex and even played the role of flow-field tracer particles.

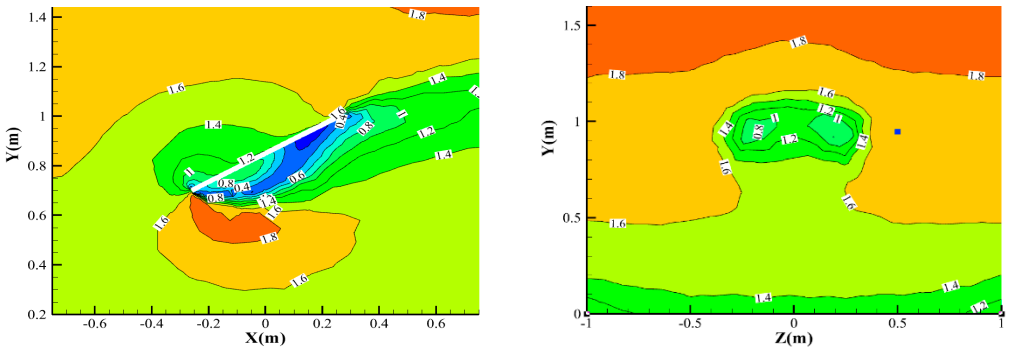
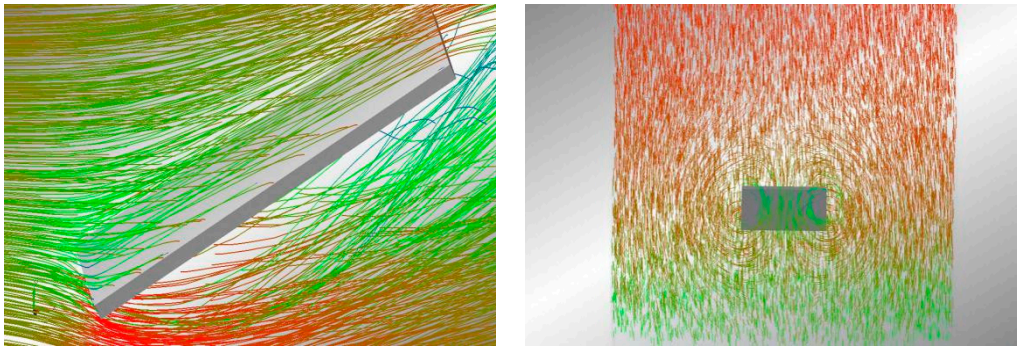


Figure 5. Velocity distribution around solar panel on different contour surfaces when $u_* = 0.1$ ms^{-1}. (**a**) z = 0 m (**b**) x = 0.5 m.

Figure 7 shows the statistical results of the total amount of dust deposition on the solar panel. It can be seen from the figure that the amount of dust deposition on the solar panel was about 14,000 particles per second, and the deposition rate (the number of particles deposited divided by the release number within the same windward area) was about 4.6%. Our simulation results showed that the amount of dust deposition increased linearly with time. Thus, it was calculated that the actual settlement mass of 10 μm dust on the solar

panel after 24 h was 4.64 g/m^2, which was comparable to the field measurement result (2.5 g/m^2/day) of Sayigh [30]. In addition, considering the results of Figure 3, it was concluded that the 10 μm dust particles were easy to deposit on the solar panel when the wind speed was small. Similar results have also been reported by Dagher et al. [23]. In addition, because the small wind speed was more conducive to dust accumulation, we also inferred that dusty weather will cause a large number of small dust particles to deposit on the solar panel. However, the negative effect of dust accumulation on the PV panels dedicated to railway power supplies could be reduced by increasing its installation height.



(**a**) (**b**)

Figure 6. Movement of dust particles with particle size of 10 μm around the solar panel, $u_* = 0.25$ ms^{-1}, $K = 0.5 \times 10^6$ Jm^{-3}. (**a**) Side view. (**b**) Back view.

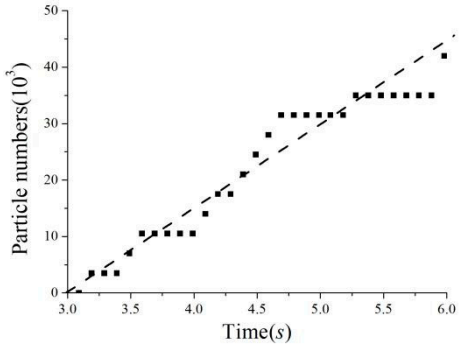


Figure 7. The total number of particles deposited on the solar panel.

3.2. Deposition Characteristics of Fine Sand Particles on Solar Panels

The deposition process of fine sand with a particle size of 100 μm under flow with a fixed friction velocity of $u_* = 0.25$ m/s was discussed, for which the dust particles were released along the x-direction, the initial particle velocity obeyed a normal distribution with a mean $\overline{v} = 3$ m/s and a standard deviation $\sigma = 1.5$ m/s, and the calculation time step was 3.0×10^{-7} s. According to Shao et al. [29], it can be assumed that the concentration of 100 μm particles in dusty weather with 1 km visibility is 0.62 mg/m^3. Then, given that $U = 3$ m/s, $m = 1.07 \times 10^{-3}$ mg and by following Formula (11), the number of dust particles entering from the entrance section per unit time was 1.043×10^4/s. When $K = 0.5 \times 10^6$ J/m^3, the results of the particle deposition number vs. velocity at different times are shown in Figure 8. From this, we can see that at the beginning of the coupling calculation (0.02 s, Figure 8a), the particle velocity basically followed a normal distribution, but after 0.2 s and 1.0 s through the acceleration of air flow, the high-speed dust particles accounted for a larger proportion (Figure 8b,c). However, the influence of the flow field around the solar panel and the impact of the dust particles on the ground and on the solar panel caused the number–velocity histogram to become irregular. It is particularly noteworthy that there were some particles that were basically at rest, such as the dust particles that stayed on the panel after the dust particles hit the solar panel, as shown in

Figure 8d. Figure 9 shows the settlement of 100 μm sand particles on the solar panel. It can be seen that there were indeed some dust particles deposited on the solar panel. Due to the short simulation time, the deposition amount was less.

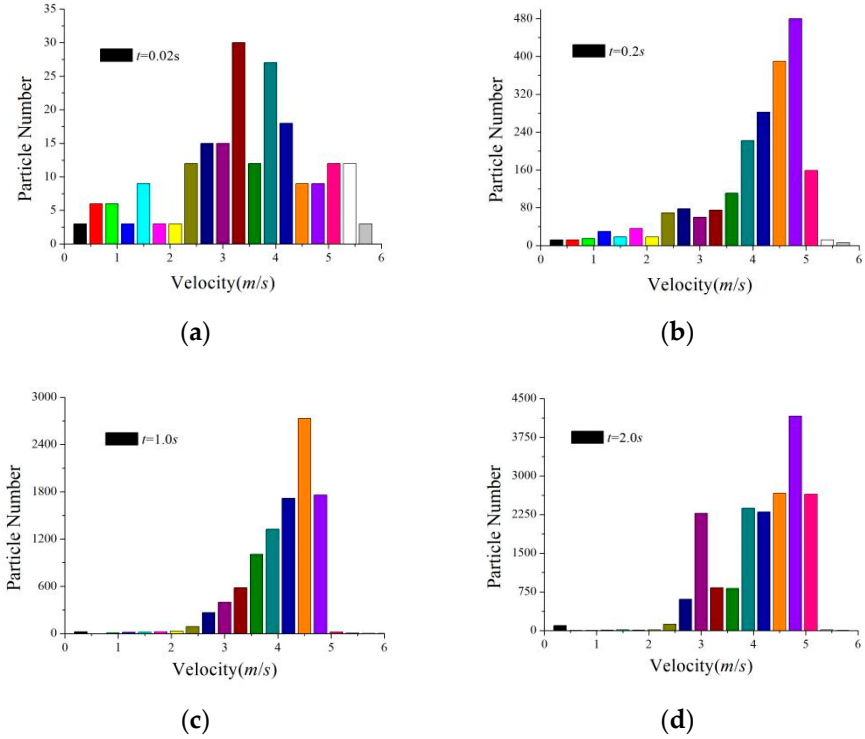


Figure 8. Velocity distribution of fine particles at different times in the flow field.

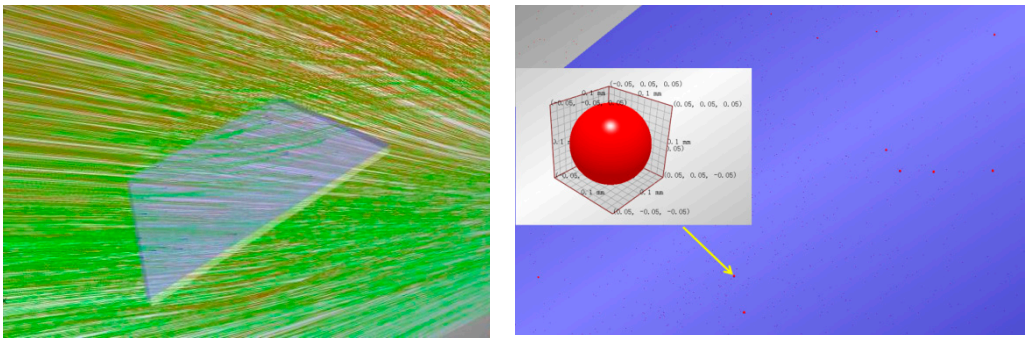
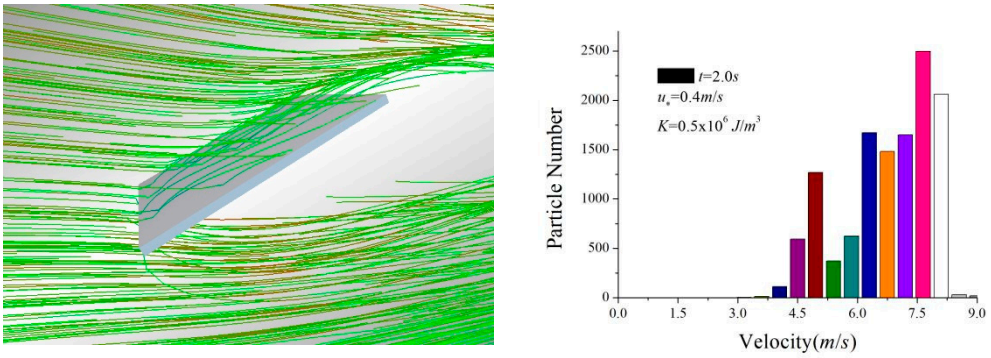


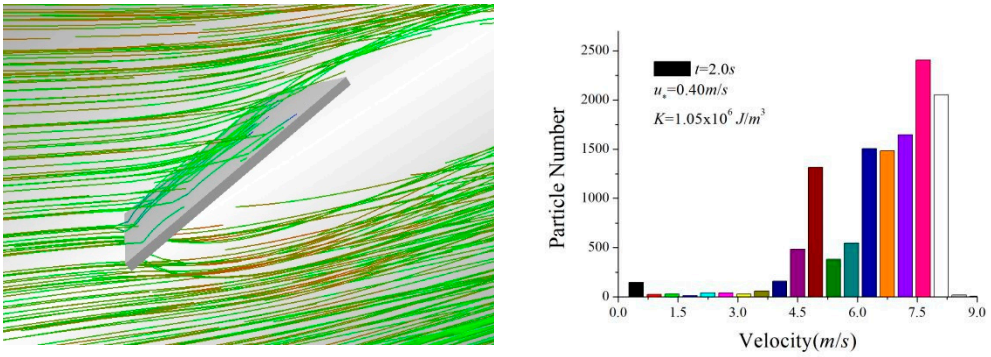
Figure 9. Movement of dust particles around solar panel. (**left**) Particle streamlines; (**right**) dust particles settled on the solar panel, where the red point indicates dust particles.

For 100 μm fine sand, increasing the wind speed led to an increasing in the speed of the sand impacting the solar panel. Figure 10 shows the streamlines of the sand particles around the solar panel and the number of particles deposited on the panel surface. We chose that $u_* = 0.40$ m/s and $K = 0.5 \times 10^6$ J/m^3. From Figure 10a, it can be seen that the dust particles basically rebounded after hitting the solar panel, and few particles were deposited on the panel surface after 2 s, as shown in Figure 10b. Therefore, due to the weak cohesion force between the sand particles and the PV glass panels, the fine sand particles could deposit on the solar panel at low wind speeds, but it would be difficult for them to be deposited when the wind speed increases. This phenomenon has also been reported by Dagher [23]. For medium and stronger cohesion forces, the deposition of fine sand particles was different, which can be seen from Figures 11 and 12, where the fine sand particles could also be deposited on the solar panel at the same time with less rebound.



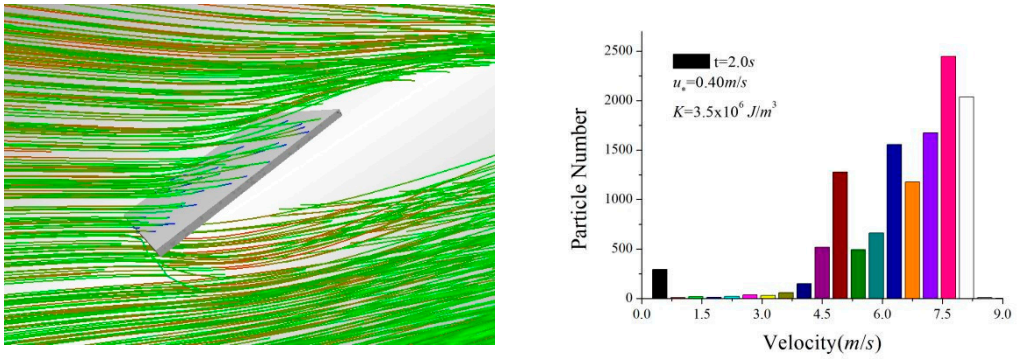
(**a**) (**b**)

Figure 10. Movement of dust particles with a particle size of 100 µm around solar panels when $u_* = 0.40$ m/s and $K = 0.5 \times 10^6$ Jm^{-3}. (**a**) Particle streamlines. (**b**) Velocity distribution of particles at 2.0 s.



(**a**) (**b**)

Figure 11. Movement of dust particles with a particle size of 100 µm around solar panels when $u_* = 0.40$ m/s and $K = 1.05 \times 10^6$ Jm^{-3}. (**a**) Particle streamlines. (**b**) Velocity distribution of particles at 2.0 s.



(**a**) (**b**)

Figure 12. Movement of dust particles with a particle size of 100 µm around solar panels when $u_* = 0.40$ m/s and $K = 3.5 \times 10^6$ Jm^{-3}. (**a**) Particle streamlines. (**b**) Velocity distribution of particles at 2.0 s.

The number of deposited sand particles on the different parts of the solar panel were changed into distribution data; then, a cloud chart of the number of particles was drawn based on the data, see Figure 13. Figure 13 shows the concentration distribution of fine sand particles deposited on the solar panel in a day when $u_* = 0.40$ m/s and $K = 3.5 \times 10^6$ J/m^3, for which we can see that along incline of the solar panel, the concentration gradually decreased. This phenomenon meant that the dust deposition on the photovoltaic panel was

not uniformly distributed, which may have been caused by the rolling down of the fine sand grains from the upper part of the solar panel. It is well known that dust deposition can reduce the amount of sunlight that a PV cell senses, thus affecting the efficiency of photovoltaic cells to generate electricity. A non-uniform distribution of dust also acts as a local shield for photovoltaic cells, which can have a negative impact on the efficient operation of photovoltaic cells. The larger concentration at the lower part of the solar panel may have been caused by the continuous rolling down of sand particles from the upper part. When using compressed air to remove dust depositions from photovoltaic panels [31], one should pay attention to this phenomenon to ensure the efficiency of the dust removal.

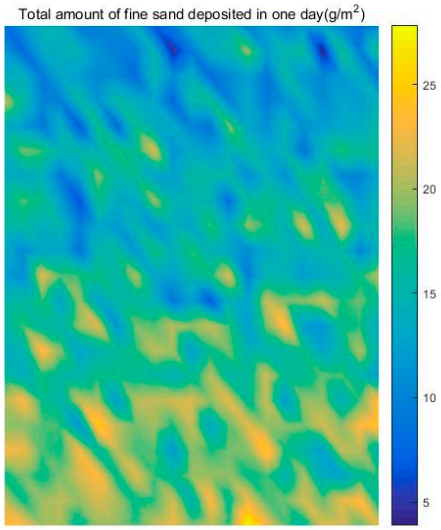


Figure 13. Cloud chart of particles deposited on solar panel in a day with a particle size of 100 um when $u_* = 0.40$ m/s and $K = 3.5 \times 10^6$ Jm^{-3}.

Figure 14 discusses the effects of the wind speed and the cohesion parameter, K, on the deposition amount of fine sand on the solar panel surface. It can be seen that under a small wind speed, the total amount of particle deposition increased with the increase in cohesion, but eventually tended to a fixed value, while under a large wind speed, the total amount of particle deposition increased with the increase in cohesion. Figure 14b shows that the deposition of particles was significantly reduced with the increase in the wind speed with weak and moderate cohesion, which indicated that a low wind speed was more favorable for deposition on the photovoltaic panel surface, and the rebound ratio of particles on the solar panel surface was larger under a high wind speed. Meanwhile, for strong cohesion, the deposition rate was almost the same for the small and large wind velocities (32% and 30%). From Figure 14b, it can be seen that the settlement number of fine sand particles on the solar panel was about 72~165 per second, i.e., about 48.3~107 g/m^2 after a week. According to the attenuation curve of the radiation intensity of a solar panel covered with 80 μm dust particles given by El Shobokshy [9] the radiation intensity reduces by 10–20%, corresponding to the above amount of dust deposition.

3.3. Light Transmittance

The deposition of dust on a solar panel will lead to the attenuation of light transmittance. According to Lambert–Beer law, the light transmittance through a certain medium can be given by the following formula [32]:

$$T = \exp[-(1-\gamma)N_s A] \tag{13}$$

where γ is the transparency of particles. For sand particles, it can be taken as $\gamma = 0.45$. N_s is the number of sand particles deposited per unit area and A is the cross-sectional area of sand dust particles. Figure 15 shows the change in the light transmittance with

time due to the deposition of dust and fine sand on the solar panel. It can be seen that the light transmittance gradually decreased with the development of time, which was basically consistent with the field measurement results reported by Saidan et al. [14].

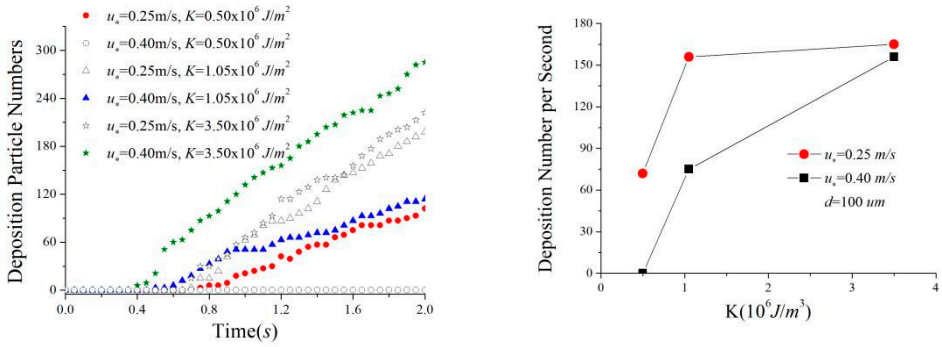


Figure 14. Comparison of the settlement amount and deposition rate of fine sand particles with different cohesion parameters and wind speeds. (**left**) Settlement amount. (**right**) Dust deposition rate.

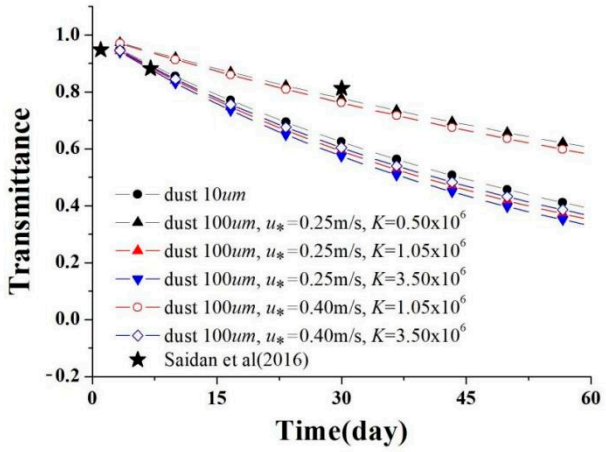


Figure 15. Change in light transmittance with time in dusty environment.

4. Conclusions

In this paper, the CFD–EDM method was used to simulate the deposition process of dust (10 μm) and fine sand (100 μm) on a solar panel under the conditions of airflow. Different from the research of [22,33], the soft sphere model and the CFD–EDM method were applied in this work, which was used to simulate in detail the interactions between dust and a solar panel so that the deposition and rebound behavior of the dust particles on the solar panel would be more believable than the rebound or deposition before simulation. For the deposition of dust particles, the simulation results showed that most of them bypassed the solar panel with the air flow, and few dust particles could settle on the surface of the solar panel (the deposition rate was only 4.6%), while the deposition rate of fine sand was relatively large (up to 32%). In the case of the fine sand deposition, the deposition number per second decreased with the increase in the wind speed in the case of weak and medium cohesion forces due to more rebounding particles, but for the case of strong cohesion forces, the deposition rate was basically unchanged, which was mainly because the rebound rate of fine sand reached a minimum. These results are of great scientific significance for understanding the law of dust deposition on photovoltaic panels.

Author Contributions: Conceptualization, J.Z. and X.L.; software, J.Z. and L.Q.; investigation, X.L.; writing—original draft preparation, J.Z. and J.W.; writing—review and editing, X.L. and Juan Wang. All authors have read and agreed to the published version of the manuscript.

Funding: This research was financially supported by the National Natural Science Foundation of China (12064034), the Leading Talents Project of Science and Technology Innovation in Ningxia Province in China (2020GKLRLX08), the Natural Science Foundation of Ningxia Province (2022AAC03117), the Department of Education Jiangsu Province | Natural Science Research of Jiangsu Higher Education Institutions of China (19KJB560005), the Major Science and Technology Project of Ningxia Autonomous Region (2022BDE03006), and the Fundamental Research Funds for the Central Universities, Lanzhou University (lzujbky-2022-kb08).

Institutional Review Board Statement: Not applicable.

Informed Consent Statement: Not applicable.

Data Availability Statement: All the correlated data are available on request from the author Jinghong Zhang.

Conflicts of Interest: The authors declare no conflict of interest.

Nomenclature

t *Time*
x_j The j-th component of coordinate
y The vertical coordinate of the calculation region
ρ_a, μ_a the air density and dynamic viscosity coefficient
E_i the elastic modulus of contacted spheres: i = 1,2
v_i Poisson's ratio of contacted spheres, i = 1,2
G_i the shear modulus of contacted spheres, i = 1,2
e the recovery factor
β correction factor of contact force
π circular constant
K the adhesion energy density
y_0 the roughness height
ρ fluid density
$\overline{u}_i$ the i-th component of time-averaged velocity
f_i the i-th component of acceleration
R_{ij} Reynolds stress
τ_{ij}^m molecular viscosity stress
S_{ij} velocity gradient
k turbulence kinetic energy
ε turbulence dissipation rate
m_i mass of the ith particle
$\vec{v}_i$ velocity of the ith particle
$\vec{f}_{drag,i}$ the drag force of particle
$\vec{g}$ gravitational acceleration
A_b the projected area of dust particle
d_p the diameter of particle
s at the inlet
T the light transmittance through a certain medium
γ the transparency of particles
N_s the number of sand particles deposited per unit area
c the mass concentration of sand and dust
$\vec{v}_{p-a}^{rel}$ the relative velocity between particles and air flow
C_d the drag coefficient
Re Reynolds number
$\vec{F}_n$ the normal force of particle
$\vec{F}_{nd}$ the normal damping force of particle
$\vec{F}_\tau$ the tangent damping force of particle
F_{nc} the normal cohesion force
α the normal overlap of two contact particle
R_1,R_2 the radius of the two contact particle
m_1, m_2 the mass of the two contact particle
D_{12} the distance between the centers of two spheres
E^* the equivalent modulus of elasticity
R^* the equivalent radius
m^* the equivalent mass
v_n^{ref} the normal component of relative velocity
S_n the normal stiffness
S_t the tangential stiffness
G^* the equivalent shear modulus
A the contact area of two contacted particles
$u(y)$ the longitudinal wind velocity
u_* the friction wind velocity
N the particle number of dust entering from the entrance section in unit time
A the cross-sectional area of flow field area
U the average speed at inlet
$\overline{v}$ the mean release velocity of particles at the inlet
σ the standard deviation of the release velocity of particle

References

1. Ning, F.; Ji, L.; Ma, J.; Jia, L.; Yu, Z. Research and analysis of a flexible integrated development model of railway system and photovoltaic in China. *Renew. Energy* **2021**, *175*, 853–867. [CrossRef]
2. Wamukonya, N. Solar home system electrification as a viable technology option for Africa's development. *Energy Policy* **2007**, *35*, 6–14. [CrossRef]
3. Maghami, M.R.; Hizam, H.; Gomes, C.; Radzi, M.A.; Rezadad, M.I.; Hajighorbani, S. Power loss due to soiling on solar panel: A review. *Renew. Sustain. Energy Rev.* **2016**, *59*, 1307–1316. [CrossRef]
4. Costa, S.C.S.; Diniz, A.S.A.C.; Kazmerski, L.L. Solar energy dust and soiling R&D progress: Literature review update for 2016. *Renew. Sustain. Energy Rev.* **2018**, *82*, 2504–2536. [CrossRef]
5. Costa, S.C.S.; Diniz, A.S.A.C.; Kazmerski, L.L. Dust and soiling issues and impacts relating to solar energy systems: Literature review update for 2012–2015. *Renew. Sustain. Energy Rev.* **2016**, *63*, 33–61. [CrossRef]

6. Du, X.; Jiang, F.; Liu, E.; Wu, C.; Ghorbel, F.H. Turbulent airflow dust particle removal from solar panel surface: Analysis and experiment. *J. Aerosol Sci.* **2019**, *130*, 32–44. [CrossRef]
7. El-Shobokshy, M.S.; Mujahid, A.; Zakzouk, A.K.M. Effects of dust on the performance of concentrator photovoltaic cells. *IEE Proc. I Solid State Electron Dev.* **1985**, *132*, 5–8. [CrossRef]
8. El-Shobokshy, M.S.; Hussein, F.M. Degradation of photovoltaic cell performance due to dust deposition on to its surface. *Renew. Energy* **1993**, *3*, 585–590. [CrossRef]
9. El-Shobokshy, M.S.; Hussein, F.M. Effect of dust with different physical properties on the performance of photovoltaic cells. *Sol. Energy* **1993**, *51*, 505–511. [CrossRef]
10. Salim, A.A.; Huraib, F.S.; Eugenio, N.N. PV power study of system options and optimization. In Proceedings of the 8th European PV Solar Energy Conference, Florence, Italy, 9–13 May 1988; pp. 688–692.
11. Sulaiman, S.A.; Hussain, H.H.; Leh, N.S.H.N.; Razali, M.S.I. Effects of dust on the performance of PV panels. *Int. J. Mech. Mechatron. Eng.* **2011**, *58*, 588–593.
12. Kaldellis, J.K.; Kapsali, M. Simulating the dust effect on the energy performance of photovoltaic generators based on experimental measurements. *Energy* **2011**, *36*, 5154–5161. [CrossRef]
13. Darwish, Z.A.; Kazem, H.A.; Sopian, K.; Al-Goul, M.A.; Alawadhi, H. Effect of dust pollutant type on photovoltaic performance. *Renew. Sustain. Energy Rev.* **2015**, *41*, 735–744. [CrossRef]
14. Saidan, M.; Albaali, A.G.; Alasis, E.; Kaldellis, J.K.A. Experimental study on the effect of dust deposition on solar photovoltaic panels in desert environment. *Renew. Energy* **2016**, *92*, 499–505. [CrossRef]
15. Beattie, N.S.; Moir, R.S.; Chacko, C.; Buffoni, G.; Roberts, S.H.; Pearsall, N.M. Understanding the effects of sand and dust accumulation on photovoltaic modules. *Renew. Energy* **2012**, *48*, 448–452. [CrossRef]
16. Huang, W.; Zhou, K.; Sun, K.; He, Z. Effects of wind flow structure, particle flow and deposition pattern on photovoltaic energy harvest around a block. *Appl. Energy* **2019**, *253*, 113523. [CrossRef]
17. Jubayer, C.M.; Hangan, H. Numerical simulation of wind effects on a stand-alone ground mounted photovoltaic (PV) system. *J. Wind Eng. Ind. Aerodyn.* **2014**, *134*, 56–64. [CrossRef]
18. Ogedengbe, A. Experimental Investigation of Wind Effect on Solar Panels. Master's Thesis, University of Western Ontario, London, ON, Canada, 2013.
19. Tominaga, Y.; Akabayashi, S.-i.; Kitahara, T.; Arinami, Y. Air flow around isolated gable-roof buildings with different roof pitches: Wind tunnel experiments and CFD simulations. *Build. Environ.* **2015**, *84*, 204–213. [CrossRef]
20. Ullah, A.; Imran, H.; Maqsood, Z.; Butt, N.Z. Investigation of optimal tilt angles and effects of soiling on PV energy production in Pakistan. *Renew. Energy* **2019**, *139*, 830–843. [CrossRef]
21. Lu, H.; Zhao, W. Effects of particle sizes and tilt angles on dust deposition characteristics of a ground-mounted solar photovoltaic system. *Appl. Energy* **2018**, *220*, 514–526. [CrossRef]
22. Lu, H.; Zhao, W. CFD prediction of dust pollution and impact on an isolated ground-mounted solar photovoltaic system. *Renew. Energy* **2019**, *131*, 829–840. [CrossRef]
23. Dagher, M.M.; Kandil, H.A. Computational prediction of dust deposition on solar panels. *Environ. Sci. Pollut. Res.* **2022**. [CrossRef] [PubMed]
24. Yu, H.; Cheng, W.; Wu, L.; Wang, H.; Xie, Y. Mechanisms of dust diffuse pollution under forced-exhaust ventilation in fully-mechanized excavation faces by CFD-DEM. *Powder Technol.* **2017**, *317*, 31–47. [CrossRef]
25. Hou, X.; Ding, T.; Deng, Z.; Yu, Z.; Xue, P.; Cao, P.; Tang, T. Study of the creeping of irregularly shaped Martian dust particles based on DEM-CFD. *Powder Technol.* **2018**, *328*, 184–198. [CrossRef]
26. Wen, C.Y.; Yu, Y.H. Mechanics of Fluidization. *Chem. Eng. Prog. Symp. Ser.* **1966**, *62*, 100–111.
27. Yang, W.; Meng, W.; Gao, L.; Tan, Y.; Fottner, J.; Dai, X.; Yao, F.; Yuan, Y.; Sun, X. Analysis of the Screw Flight Wear Model and Wear Regularity of the Bulk Transport in Screw Ship Unloader. *Iran. J. Sci. Technol. Trans. Mech. Eng.* **2022**, *46*, 15–29. [CrossRef]
28. Isaifan, R.J.; Johnson, D.; Ackermann, L.; Figgis, B.; Ayoub, M. Evaluation of the adhesion forces between dust particles and photovoltaic module surfaces. *Sol. Energy Mater. Sol. Cells* **2019**, *191*, 413–421. [CrossRef]
29. Shao, Y.; Yang, Y.; Wang, J.; Song, Z.; Leslie, L.M.; Dong, C.; Zhang, Z.; Lin, Z.; Kanai, Y.; Yabuki, S.; et al. Northeast Asian dust storms: Real-time numerical prediction and validation. *J. Geophys. Res. Atmos.* **2003**, *108*, 4691. [CrossRef]
30. Sayigh, A.A.M. Effect of dust on flat plate collectors. In Proceedings of the International Solar Energy Society Congress, New Delhi, India, 16–21 January 1978; pp. 960–964.
31. Li, D.; King, M.; Dooner, M.; Guo, S.; Wang, J. Study on the cleaning and cooling of solar photovoltaic panels using compressed airflow. *Sol. Energy* **2021**, *221*, 433–444. [CrossRef]
32. Li, X.; Niu, K. Effectively predict the solar radiation transmittance of dusty photovoltaic panels through Lambert-Beer law. *Renew. Energy* **2018**, *123*, 634–638.
33. Lu, H.; Zhang, L.-Z. Influences of dust deposition on ground-mounted solar photovoltaic arrays: A CFD simulation study. *Renew. Energy* **2019**, *135*, 21–31. [CrossRef]

Disclaimer/Publisher's Note: The statements, opinions and data contained in all publications are solely those of the individual author(s) and contributor(s) and not of MDPI and/or the editor(s). MDPI and/or the editor(s) disclaim responsibility for any injury to people or property resulting from any ideas, methods, instructions or products referred to in the content.